Simplify your imaging workflows

Make research imaging workflows accessible, traceable, and secure with Athena Software for Core Imaging Facilities.

Thermo Scientific™ Athena Software is a premium imaging data management platform designed for core imaging facilities that support materials science research.

Athena Software ensures traceability of images, metadata, and experimental workflows through an intuitive and collaborative web interface.

Find out more at **thermofisher.com/athena**

ThermoFisher SCIENTIFIC

ADVANCED FUNCTIONAL MATERIALS
www.afm-journal.de

Perfectly Aligned, Air-Suspended Nanowire Array Heater and Its Application in an Always-On Gas Sensor

*Kwang-Wook Choi, Min-Seung Jo, Jae-Shin Lee, Jae-Young Yoo, and Jun-Bo Yoon**

In spite of the excellent thermal properties of nanowires, the typical form factor of unrefined nanowires has restricted their potential use in developing ultralow power electrothermal heater and application device. In this paper, a nanowire array with a perfectly aligned geometric structure on an air-suspended beam is proposed as a novel heating element. By locally confining the generated heat and suppressing beam conduction loss to the substrate, the proposed nanowire array heater overcomes the fundamental power consumption limits of conventional film-type microheaters. As a result, only 2.51 mW of power is required to reach an average temperature of 300 °C, surpassing the performance of state-of-the-art microheaters. The developed nanowire array heater is monolithically integrated with gas sensing nanowires to demonstrate its full capability as an ultralow power gas sensor. The fabricated device successfully detects low concentration carbon monoxide gas of 1 ppm, using less than 5 mW of power. The presented technique offers a promising pathway toward realizing always-on gas sensors driven by battery-powered mobile devices, which will ensure a hazardous gas-free safe environment. In addition, the proposed strategy of employing geometrically structured nanomaterials in the electrothermal heater design enables to lead out their potential thermal capability in many other applications.

1. Introduction

The advent of the Internet of Things has led consumer and industrial demand for a variety of energy-efficient, high-performance micro- and nanodevices. One of the fundamental components utilized in various functional devices is electrothermal heaters, which provide the thermal energy required to operate heater-based devices, such as infrared emitters,[1,2] air-flow sensors,[3,4] and gas sensors.[5,6] In this regard, nanowires have received particular attention as a promising building block in advanced electrothermal heaters, where extraordinary thermal characteristics are essential. This is because the thermal properties of nanowires have distinct advantages compared to microscale counterparts. The thermal conductivity of nanowires is drastically reduced due to the increased scattering of electrons/phonons at nanoscale surfaces.[7–9] In addition, the inherent small geometries of nanowires act as barriers against heat conduction, effectively confining the heat within a localized region.[10] Meanwhile, the high aspect ratio of nanowires provides a stable current path in the long axis. These advantages make nanowires excellent constituents of ultralow power electrothermal heaters, which can replace the conventional film-type microheaters.

Nevertheless, the unique thermal properties of nanowires have not yet been fully exploited. To date, studies of nanowires in electrothermal heaters have primarily focused on other characteristics, such as flexibility or transparency.[11–14] The major hurdle that restricts the potential capability of nanowires has been their form factor. The most widely used form is randomly distributed nanowires dispersed on a processing substrate. However, these random networks inevitably create unpredictable junctions between nanowires, which undermines precise controllability.[15] In addition, the substrate in contact with nanowires acts as a huge heatsink, significantly lowering the power efficiency of the device.[16] Above all, the undesirable form factors make it difficult to integrate functional materials on the nanowire heaters, which severely limits their fields of application.

Here, we incorporate the nanowires into a perfectly aligned, air-suspended array to make the best use of their unique thermal properties. Recent advances in nanofabrication technologies have made it possible to study the geometric effect of nanomaterials, which can further improve device performance.[17] The proposed geometry allows us to explore the optimized design of heaters, which leads out the potential thermal capability of the nanowires. In particular, we focused on their ability to confine heat in a localized region, thereby suppressing beam conduction loss to the substrate. It should be noted that beam conduction loss imposes a fundamental limit on the power consumption of conventional film-type microheaters. Based on a theoretical assumption that considered the dominant heat loss mechanism, we demonstrated that a perfectly aligned nanowire array located on an optimally designed air-suspended beam could greatly enhance the energy efficiency of the heating element. The developed nanowire array heater consumed only 2.51 mW to reach 300 °C, surpassing the performance of similar-sized film-type microheaters.[18–20] In other words, thanks to the geometric structuring, the advantageous

K.-W. Choi, M.-S. Jo, J.-S. Lee, Dr. J.-Y. Yoo, Prof. J.-B. Yoon
School of Electrical Engineering
Korea Advanced Institute of Science and Technology (KAIST)
291 Daehak-ro, Yuseong-gu, Daejeon 34141, Republic of Korea
E-mail: jboon@kaist.ac.kr

The ORCID identification number(s) for the author(s) of this article can be found under https://doi.org/10.1002/adfm.202004448.

DOI: 10.1002/adfm.202004448

thermal properties of the nanowires could be fully exploited, overcoming the fundamental power consumption limit of conventional electrothermal heaters.

The developed nanowire array heater was then successfully applied in ultralow power semiconducting metal-oxide (SMO) gas sensors. Metal-oxides are functional materials that can be used to detect harmful gases in the atmosphere, by observing changes in their resistance at elevated temperatures. In this study, gas sensing metal-oxide in the form of perfectly aligned nanowires as well was monolithically integrated with the nanowire array heater. The monolithic structure enabled precise and uniform device fabrication, which is differentiated from conventional integration forms of randomly distributed nanomaterials. The heater provided the temperature required to activate the gas sensing mechanism with power consumption of less than 5 mW, and the sensor detected low concentration of carbon monoxide (CO) gas of 1 ppm. The achieved power is one of the lowest levels among state-of-the-art SMO gas sensors.[21–25] It has been strongly desired to develop always-on gas sensors that are implementable in mobile devices to ensure a gas-hazard free environment everywhere in daily life. The ultralow power performance, achieved with geometrically structured nanomaterials, confirms this is a promising nanotechnology for realizing always-on gas sensors in power-stringent mobile devices.

2. Results and Discussion

Figure 1 represents the proposed design of the ultralow power nanowire array heater compared with conventional film-type microheaters. To take full advantages of the excellent thermal properties of nanowires, it is important to understand a dominant heat loss mechanism of electrothermal heaters and conventional approaches for lowering the power consumption. An air-suspended double-clamped beam (Figure 1,i) has been the most widely adopted structure for the ultralow power microheaters, because it provides excellent thermal isolation with minimal heat conduction path.[24] The effective way to lower the power consumption so far has been downscaling the heating area. To be specific, considering the critical dimensions of the applied lithography tools and the mechanical strength of the air-suspended structure, the width and thickness of the beam are generally set to be as small as possible, while beam lengths are varied to control the heating area. However, the downscaling approach encounters its limit in terms of energy efficiency. Although air conduction loss of microheaters decreases proportionally with decreasing heating area, beam conduction loss through the substrate can greatly increase as the distance between the beam and anchor decreases.[22,26] In other words, there is an optimum point at which the two major sources of heat loss are balanced (Figure 1,ii). Shorter beam lengths than the optimum point result in disproportionately larger heat loss through the beam compared to the decrease in heat loss to the air. Conclusively, the increasing beam conduction loss during the downscaling process has imposed a fundamental limit on lowering the power consumption. Here, to address the aforementioned challenges, a novel geometrical structure of nanowires was developed; the perfectly aligned nanowire array was employed as a basic heater element and located on an air-bridged beam devised for separating the heating area from the anchor (Figure 1,iii). The unique thermal properties of nanowires combined with the air-bridge structure can greatly suppress beam conduction loss to the substrate by locally confining the generated heat only to the air-bridged beam. As a result, the minimum amount of heat loss achievable with optimum design can be even further reduced by shifting the optimum point to a smaller size (Figure 1,iv). The theoretical assumption was supported by experimental results, which will be presented later.

The fabrication process of the proposed nanowire array heater is schematically illustrated in **Figure 2**a, with more details provided in Figure S1 of the Supporting Information. The most widely used bottom-up approach of synthesizing nanowires is not suitable in this study, because it leads to difficulty in aligning and locating the nanowires in a desirable

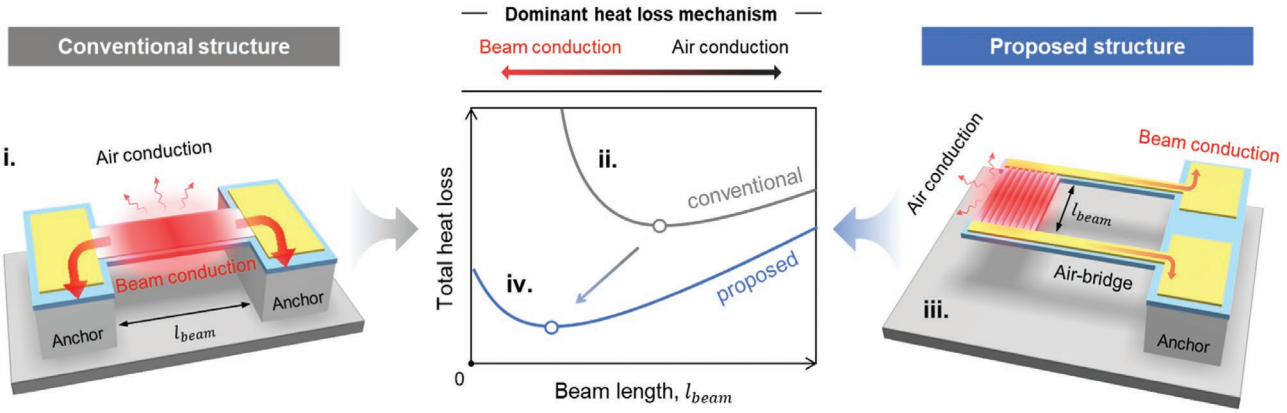

Figure 1. Overview of proposed nanowire array heater and theoretical explanation of dominant heat loss mechanism. Schematics of conventional film-type, double-clamped beam microheater (i), and proposed nanowire array heater with the air-bridge structure (iii). Magnitude and direction of heat loss through beam conduction are visualized by red arrows, and heat loss through air conduction is represented with wavy arrows. Center graph shows size-dependent total heat loss curves (virtual) for comparison of conventional structure (ii) and proposed structure (iv). Optimum beam length, where beam conduction and air conduction loss are balanced, as well as total heat loss, can be decreased with the proposed structure. Optimum points are marked with open dots.

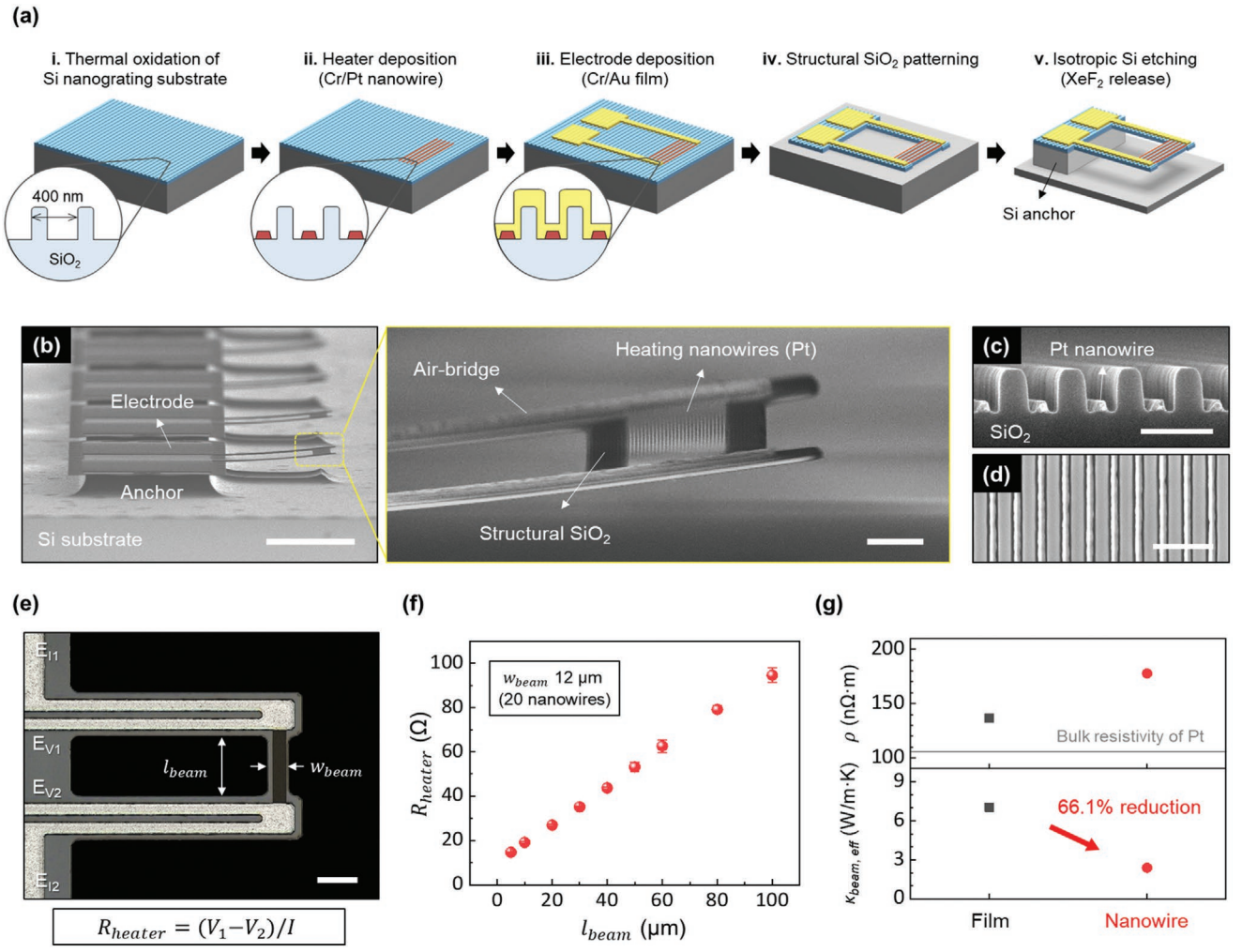

Figure 2. Fabrication of the nanowire array heater and its electrical and thermal characteristics. a) Schematic presentation of fabrication procedures. b) Scanning electron microscope (SEM) images of the fabricated device in projected view. c) Cross-section and (d) top-view SEM images of heating nanowires (Pt) on structural SiO_2. e) Top view laser scanning microscope image to show electrode configuration for electrical measurements. f) Measured electrical resistance with various beam lengths. Width of beam was 12 μm for all measurements. g) Extracted resistivity of Pt and effective thermal conductivity of beam depending on structures of heating element. (Scale bars: (b) left-100 μm, right-10 μm, (c) 500 nm, (d) 1 μm, (e) 20 μm.)

manner. The unique nanostructure was realized by developing a sophisticated top-down approach. First, a periodic Si nanograting (NG) substrate with 80 nm linewidth and 320 nm spacing is prepared,[27,28] followed by thermal oxidation. The oxidized NG with 500 nm in thickness serves as a structural mold for nanowire fabrication as well as a robust mechanical support after its air-suspension. The strategy for fabricating a perfectly aligned nanowire array is to deposit the heater material only at the valleys of the NG by employing a sacrificial shadow pattern (SSP).[29] The SSP formed on the protruding part of NG is removed after the heater material is deposited. In this way, only the nanowires remain in the valleys of the NG (Figure S1b, Supporting Information). Two consecutive lift-off patterning processes are conducted to define heater and electrode area, respectively. Here, 80 nm thick Pt is used as the heater material and 500 nm thick Au is used as the electrode material. A thin layer of Cr (10 nm) is used as an adhesion layer for both materials. Following a SiO_2 NG patterning process to define the structural area of the device, the Si substrate is selectively etched by a final XeF_2 release process, an isotropic dry etching process that has similar vertical and lateral etch rates. The narrow part of the structural layer is air-suspended as underlying Si is totally removed, whereas a wide region is left as an anchor. The detailed fabrication process conditions can be found in the Experimental Section. Figure 2b–d shows scanning electron microscope (SEM) images of the fabricated device. The air-bridge electrically connects the nanowire array and thermally isolates the heating area from the anchor. The slight upward bending of the air-bridge can be explained by the difference in residual stress between the Au electrode and structural SiO_2. However, the free displacement rather improves the mechanical stability by preventing large stress to accumulate at the structural beam, compared with the conventional case of the double-clamped beam structure (Figure S2, Supporting Information). It should be noted that, with the aid of the structural SiO_2, Pt nanowires located on the air-bridged

beam maintain their perfect alignment. The width (diameter) of individual nanowires, measured by high magnification SEM, was 80.8 ± 3.7 nm.

It is important to investigate electrical and thermal properties of nanowires, which are different from those of microscale structures. Because the dimension of the nanowires is comparable to that of the electron mean free path, the size-dependent electron–phonon effect should be considered. The thermal conductivity κ and the electrical conductivity σ are coupled via the Wiedemann–Franz law $\kappa/\sigma = LT$ (L = Lorenz number, T = absolute temperature), which is also valid for nanoscale metal.[30,31] Therefore, the thermal conductivity of nanowires can be experimentally determined from the electrical conductivity. Here, the electrical resistance of Pt nanowires was extracted using a four-terminal measurement scheme, as illustrated in Figure 2e. DC bias current was applied through E_{I1} and E_{I2}, and the voltage drop across the nanowires was measured through E_{V1} and E_{V2}. The proportional relation of the heater resistance to the beam length (Figure 2f) verifies the reliable and controllable nanofabrication technique developed in this work. Based on the measurements, the electrical conductivity of nanowire and the effective thermal conductivity of the beam ($\kappa_{beam,\ eff}$) were sequentially calculated by taking into account the dimensions of the nanowires and the structural beam (Figure 2g). An identical thickness Pt film was also prepared for comparison. The $\kappa_{beam,\ eff}$ of the nanowire heater (2.39 W m^{-1} K^{-1}) was reduced by 66.1% compared to the film heater; this was achieved due to the decreased thermal conductivity and excellent heat confinement of the nanowires. This makes the perfectly aligned nanowire array a promising heater element for overcoming heat loss through beam conduction.

The effect of employing perfectly aligned nanowire array and the air-bridge on reducing beam conduction loss, which in turn lowers the power consumption of the heater, was systematically evaluated. **Figure 3**a shows three types of heater configurations prepared for the analysis: film and nanowires on typical double-clamped beams, and nanowires on an air-bridged beam. For each configuration, an optimal design that balances the two major sources of heat loss (through beam and air) can be found by evaluating heaters with various beam lengths. In the analysis, the width of the beam and the length of the air-bridge were fixed at 12 and 100 µm, respectively. The width of the beam was set as a minimum considering the critical dimensions and alignment margin of applied photolithography. On the other hand, structural stability and power efficiency were taken into account when determining the length of the air-bridge. Finite element simulation (Figure S3, Supporting Information) predicts that air-bridges longer than 100 µm will have only a minor effect in reducing the power consumption of the heater, whereas it becomes more difficult to ensure structural stability. The power consumption required for heaters to reach average temperature (T_{avg}) of 300 °C was experimentally extracted and is shown in Figure 3b. A resistance-temperature detector method that correlates heater resistance with temperature was applied

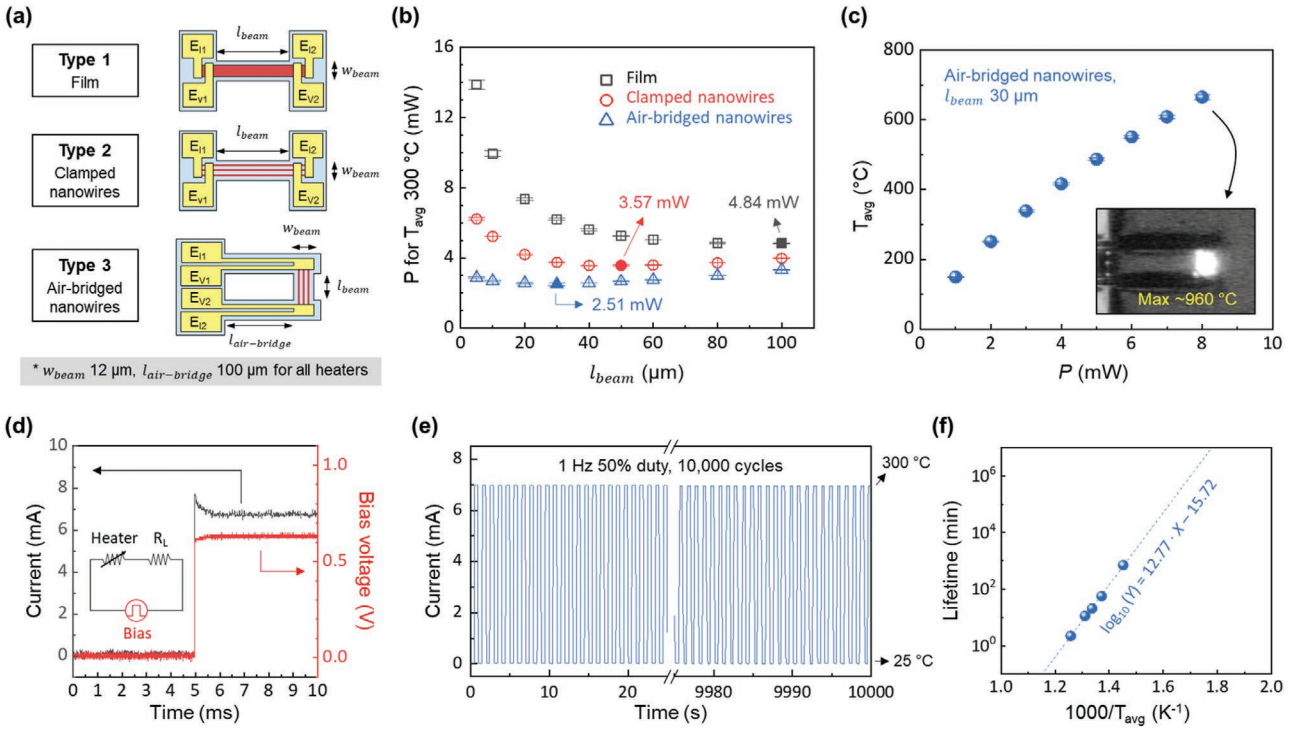

Figure 3. Heater performance characterization. a) Three-types of heater configurations prepared for comparison of power consumption. b) Evaluation of power consumption required for heaters to reach average temperature (T_{avg}) of 300 °C. Optimal point for each configuration, where beam length balances total heat loss (minimum power required), filled with color. Data in (c)–(f) were obtained from optimally designed nanowire array heater with air-bridge structure. c) Estimated temperature versus applied power. Inset shows optical image of glowing device biased at 8 mW. d) Evaluation of heating speed, and (e) repeatability of operation. Heater was biased for T_{avg} 300 °C. f) Accelerated life testing with various operating temperatures. Dashed line is extrapolated Arrhenius plot for lifetime estimation.

to estimate the operating temperature (Figure S4, Supporting Information). Comparison between film and nanowires on a double-clamped beam clearly verifies the superior thermal property of nanowires. The reduced $\kappa_{beam,\ eff}$ of nanowire heaters allows a shorter optimal beam length, which also reduces total amount of heat loss. Consistent with theoretical expectations, the increase of the input power below the optimal beam length is caused by disproportionately larger heat loss through the beam compared to the decrease in heat lost to the air. An analytical heat loss model[26] well matched our experimental results (Figure S5, Supporting Information). The improvement of power efficiency was more pronounced when nanowires were located on the air-bridged beam instead of on the typical double-clamped beam. The extended heat conduction path by the air-bridge effectively isolates the heating area from the anchor. As a result, the power consumption was reduced down to 2.51 mW (T_{avg} 300 °C) with a shortened optimal beam length of 30 µm. The achieved power is the lowest level compared with those of conventional microheaters having similar heating areas. It should be noted that the minimum required power for the film and nanowires heater on a typical double-clamped beam were 4.84 and 3.57 mW, respectively. The power consumption values decreased by 47.3% and 29.7%, respectively. Therefore, the conventional limit on lowering the power consumption, which arises from beam conduction loss, was successfully overcome using the proposed approach.

The heating capability of the optimally designed nanowire array heater with the air-bridge structure was evaluated in various aspects. Figure 3c presents the estimated temperature (T_{avg}) of the heater according to the applied power. Only 0.57 mW was required for the initial 100 °C heating, which again proves the excellent power efficiency of the nanowire array heater. Additionally, the maximum allowable power that ensures thermal stability was ≈8 mW. Under this bias condition, the heater glowed brightly (inset of Figure 3c), with the corresponding temperature at the center of the beam estimated to be ≈960 °C (Figure S6, Supporting Information). Next, a voltage pulse was applied and current through the heater was monitored to evaluate the speed of heating (Figure 3d). After step voltage input, resistance of the heater started to increase; the current decreased as temperature of heater rose over time. The heating speed, which is the time taken for the current to stabilize, was less than 1 ms (T_{avg} 300 °C). The response time was faster than those of similar microheaters, which usually have several-millisecond-level response time. This result is mainly attributed to the extremely small heat capacity of the miniaturized heating elements. In terms of practical usage, repeatability of operation is also an important characteristic because thermomechanical stress accumulating during on/off cycles may degrade heater performance. To test the repeatability of operation, the heater was biased every 1 s to undergo recurrent heating (T_{avg} 300 °C) and cooling (room temperature) cycles, as shown in Figure 3e. No observable damage could be found until the test was stopped after 10 000 cycles. The nanowire array heater showed sufficient mechanical robustness during the repeated operation cycles. Different from previous works that have used firm anchors for the heating elements,[19,32,33] thermomechanical stress even under harsh operation conditions did not result in failure of our device; rather, only electrical failures were observed (Figure S7, Supporting Information). We speculate that the air-bridge releases the thermomechanical stress of the structural beam through its free movement, effectively preventing mechanical damage. Finally, accelerated lifetime testing was carried out to evaluate the long-term reliability. A gradual increase of heater resistance was observed as electromigration progressed when device was continuously biased at high temperature (Figure S8, Supporting Information). Assuming that heater failure is mainly caused by electromigration, the temperature dependency of the lifetime can be predicted from the Arrhenius plot.[34] Here, the lifetime was defined as the point at which the initial resistance of the heater increases by 1%. In Figure 3f, the lifetime obtained at different operating temperatures is plotted as a function of $1000/T_{avg}$. The lifetime at lower operating temperature can be estimated by extrapolation, giving rise to 7.06 years for T_{avg} 300 °C. Despite using nanowires, which seem to be vulnerable to disconnection, the heater showed sufficient reliability to be applied in many commercial devices. This is attributable to the high energy efficiency of the proposed structure, which alleviates electromigration.

To widen the usage of the developed nanowire heater platform to SMO gas sensors, a sensing material should also be integrated; generated heat should be efficiently transferred so as to elevate the temperature of the gas sensing material. A novel arrangement of double-layered nanowires was employed to meet this requirement. Actually, nanowires are also a promising material for gas sensing because they have high sensitivity in responding to small concentrations of their target gases.[16,35] However, it has been difficult to manipulate conventional randomly distributed nanowires, which has made the integration process more challenging. In this work, the protruding part of NG was acutely utilized to precisely locate the perfectly aligned nanowire array right above the developed nanowire heater platform. The structure of the device incorporating gas sensing nanowires (SnO_2) with heating nanowires (Pt) is schematically shown in **Figure 4**a, and a projected view of the fabricated device is presented in Figure 4b. Detailed fabrication steps and process conditions are provided in Figure S9 of the Supporting Information and the Experimental Section.

The crucial technology for realizing the monolithic structure is to engineer cross-sectional morphology of the depositing materials, so as to selectively connect electrodes with heating and sensing nanowires. Accordingly, the beam of the double-layered nanowires consists of three distinctive sections of disparate cross-sectional morphology, as marked in Figure 4c. The first section shown in Figure 4d is the active region of gas sensor operation. The NG structure separates the SnO_2 nanowires and the Pt nanowires in the vertical direction, providing independent electrical paths. It should be noted that heterogeneous nanowires, however, are located in close proximity, so that they can efficiently transfer heat to each other. The second section shown in Figure 4e is the contact part of the Pt nanowires and heater electrodes. Conformal step coverage of the heater electrode is important to form intimate contact with Pt nanowires located in the valleys of NG. Lastly, the third section shown in Figure 4f is the contact part of the SnO_2 nanowires and the sensor electrodes. An oblique-angled deposition technique was applied to selectively contact the SnO_2 nanowires with sensor electrodes. The shadow region of the depositing

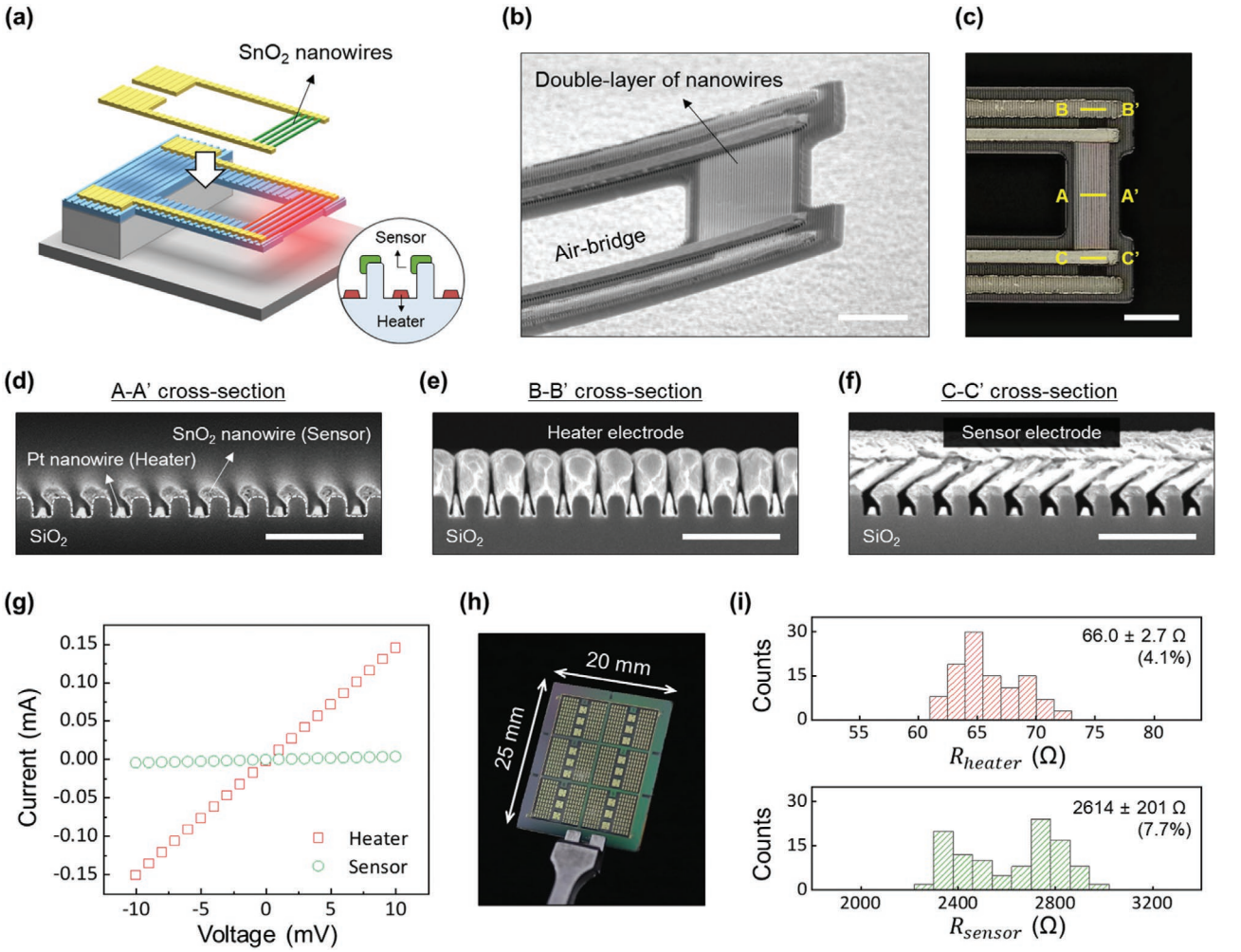

Figure 4. Fabrication of gas sensor devices monolithically integrated with the nanowire array heater. a) Schematics of proposed gas sensor device. A double-layer of nanowires with independent electrodes is employed. b) Projected view SEM image, and c) top view laser scanning microscope image of fabricated device. Three distinctive sections are marked with yellow lines. Cross-sectional SEM images of d) double-layer nanowires, e) heater electrode, and f) sensor electrode. g) Current–voltage characteristics of heater and sensor. h) Optical image of gas sensor devices bath-fabricated on inch-scale wafer. i) Evaluation of large-area uniformity represented by histograms of resistance. (Scale bars: (b) 10 µm, (c) 20 µm, (d–f) 500 nm.)

material flux prevents electrical contact with the Pt nanowires. The current–voltage characteristic of the double-layered nanowires is presented in Figure 4g. Both Pt and SnO_2 nanowires showed ohmic contact with each electrode, and their electrical conductivities were different. Note that only the noise current can flow between the heater and sensor electrodes, which ensures an independent electrical path between the heterogeneous nanowires (Figure S10, Supporting Information).

The nanofabrication technique, developed based on a top-down approach, ensures large-area uniformity. In our experiment, the gas sensor devices were batch-fabricated on an inch-scale wafer (20 mm by 25 mm), as shown in Figure 4h. For the evaluation of the uniformity, the resistances of the heater and sensor were measured from 108 different devices; the distribution of those values is plotted in Figure 4i. The degrees of deviation for the heater and sensor resistances were 4.1% and 7.7%, respectively. The broader distribution of the sensor resistance is mainly due to the deposition method applied for fabricating SnO_2 nanowires. The thickness of the SnO_2 nanowires may differ slightly by position because the distance between wafer and source material is not constant in oblique-angled deposition systems. This can be confirmed by the position dependent sensor resistance, shown in Figure S11 of the Supporting Information. Nevertheless, the obtained uniformity is superior to those of other existing nanowire devices, which is attributed to the reliable nanofabrication technique developed in this work.

Finally, fabricated device was demonstrated as an SMO gas sensor. Here, CO was chosen as the target gas to detect because it is a colorless, odorless toxic gas, which can be fatal to humans at relatively low concentrations.[24] It is important to understand that the underlying principle of operation is redox reactions of chemisorbed oxygen molecules on the surfaces of metal-oxides. Because the chemisorption takes place in the high temperature range of 190–300 °C,[36] the heater should provide sufficient temperature to the sensing layer. The schematic configuration

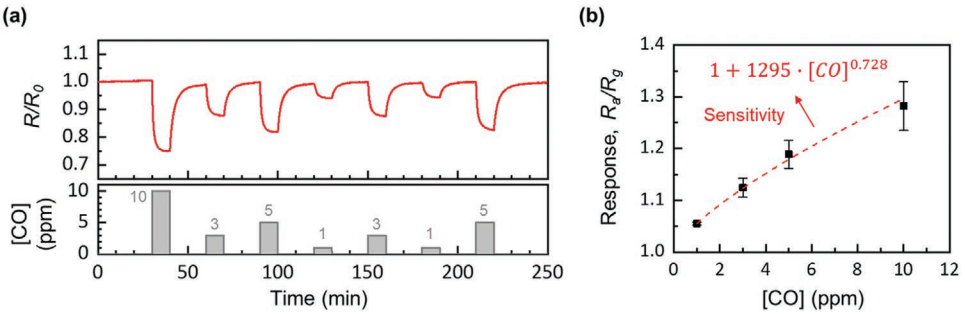

Figure 5. Gas sensor characterization. a) Transient response of sensor resistance upon exposure to arbitrary concentration of CO gas. Heater consumed 4.36 mW for measurement. b) Gas response extracted from 5 independent measurements. Dashed line represents fitted curve of sensitivity.

of the measurement setup used for the gas sensor characterization is shown in Figure S12 of the Supporting Information. The proper input power to the heater was experimentally determined. The device started to operate when the heater was biased over ≈3 mW, and it gave more sensitive and faster responses as the input power increased (Figure S13, Supporting Information). Based on the measurements, the dynamic gas sensing response to various concentrations of CO gas was evaluated, with results shown in **Figure 5**a. First, the sensor resistance decreased upon exposure to CO gas, which follows the typical response of n-type gas sensing materials to a reducing gas.[37] Second, the device was able to discriminate concentrations of CO gas, and it showed reproducible responses to the same concentrations of CO gas. The gas response, defined as R_a/R_g (R_a = sensor resistance in air, R_g = sensor resistance exposed to CO gas), is extracted in Figure 5b. The concentration of exposed CO gas can be estimated by the fitted curve of sensitivity,[38] and the device could detect concentration as low as 1 ppm. The heater consumed only 4.36 mW for this measurement. It should be pointed out that reducing the power consumption of SMO gas sensors has been a big challenge for their continuous (always-on) operation in mobile applications. We believe that the ultralow power nanowire heater platform developed in this work can provide the right solution to ever-existing challenges and finally allow implementation of always-on gas sensors in mobile devices. These new devices will alert users situated in hazardous environments in real time.

3. Conclusion

A novel geometric structure of nanowires was developed to fully exploit their unique thermal properties. The employment of a perfectly aligned nanowire array as a basic heating element, combined with an air-bridge structure, locally confined the heat only to the nanowire heater area. As a result, fundamental constraints on power efficiency arising from beam conduction loss were overcome. The ultralow power capability, as well as the mechanical stability and long-term reliability, of the nanowire array heater was verified by electrical evaluation. The heater reached an average temperature of 300 °C within 1 ms with only 2.51 mW; unprecedented ultralow power and fast heating was achieved, surpassing the performance of similar microheaters. The nanowire array heater also ensured mechanical robustness during 10 000 times of repetitive on/off cycles, and ≈7 years of a sufficient lifetime was estimated under continuous operation at 300 °C. Furthermore, for practical application, an ultralow power CO gas sensor was demonstrated by monolithically integrating the heating nanowires with the gas sensing nanowires. Using the developed monolithic process, these heterogeneous nanowires were located in close proximity, so that efficient heat transfer was guaranteed. The fabricated device successfully detected various concentrations of CO gas using less than 5 mW, which is also one of the lowest power levels ever achieved in an SMO gas sensor. Hence, the present techniques for achieving ultralow power operation offer a promising pathway toward realizing always-on gas sensors that can be implemented in power-stringent mobile devices. In addition, the proposed strategy of employing geometrically structured nanomaterials in the electrothermal heater design will provide new prospects for a variety of application devices for which ultralow power operation is strongly demanded.

4. Experimental Section

Fabrication of Nanowire Array Heaters: Si NG substrates (line width: 150 nm, space: 250 nm, height 300 nm) were prepared by krypton fluoride stepper lithography and reactive ion etching. The width of Si NG was reduced to 80 nm by repetitive chemical oxidation and etching, followed by wet oxidation in a furnace (1100 °C, 40 min: 500 nm target). SSP was employed to fabricate Pt nanowires in the valleys of the NG. The SSP was formed on the protruding parts (peaks and sidewalls) of the NG by applying two iterations of oblique-angled deposition, each at a different angle. A custom-made inclined loading chuck was used for the oblique-angled depositions. Detailed process conditions for SSP are shown in Figure S1 of the Supporting Information. After Pt deposition by e-beam evaporation (80 nm), the SSP was removed by a wet-chemical etchant. Only Pt nanowires remained in the valleys of the NG. The Pt nanowire heater was subsequently annealed in a furnace (700 °C, 3 h) to stabilize its phase under high temperature operation. The electrodes were then deposited by DC sputtering (Au, 500 nm). After patterning the structural SiO_2 by wet etching, the Si substrate was selectively removed by a final XeF_2 release process. The XeF_2 gas exposure time was modulated to obtain the desired etch profiles (XeF_2 pressure 9 mTorr).

Integration of Nanowire Sensors: NG substrates with Pt nanowires in their valleys were prepared using the method described above for heater fabrication. By applying the oblique-angled deposition method, SnO_2 nanowires formed only at the peaks of the NG. To ensure independent electrical paths from the Pt nanowires, SnO_2 was thermally evaporated with high deposition angle of 74° (50 nm). The sensor electrode should have electrical contact only with the SnO_2 nanowires. Two iterations of another oblique-angled deposition processes were conducted to form the Au electrodes (–74° 200 nm, +62° 300 nm). The purpose

of the second deposition was to lower the electrical resistance of the electrodes. Detailed fabrication processes and results are provided in Figure S9 of the Supporting Information.

Electrical Measurement: A four-terminal measurement scheme was utilized to precisely extract the heater resistance. A constant current bias was applied by a source meter (Keithley 2636B), and voltage drop was measured by a nanovoltmeter (Keithley 2182A). For the evaluation of the heating speed and the repeatability of operation, a function generator (Tabor WS8102) was used instead of the source meter.

Gas Sensor Characterization: The gas sensor devices were loaded into a sealed gas chamber, and various concentrations of CO gas were introduced to the chamber through mass flow controllers. The concentration of CO gas was adjusted by balancing the flow rates of air and CO gas. The devices in the chamber were electrically connected to a power supply and a data acquisition unit (DAQ). The power supply applied DC input to operate the heater, and DAQ (Agilent 34972A) was set to measure the sensor resistance.

Supporting Information

Supporting Information is available from the Wiley Online Library or from the author.

Acknowledgements

This research was supported by the Basic Research Program through the National Research Foundation of Korea (NRF) funded by the Ministry of Science and ICT (MSIT) (NRF-2017R1A2B3005221). This research was also supported by the KAIST UP Program. The EDA tool was supported by the IC Design Education Center (IDEC).

Conflict of Interest

The authors declare no conflict of interest.

Keywords

air-suspended nanowires, gas sensors, geometrically structured nanomaterials, perfectly aligned nanowires, ultralow power

Received: May 23, 2020
Published online: August 12, 2020

[1] A. Lochbaum, Y. Fedoryshyn, A. Dorodnyy, U. Koch, C. Hafner, J. Leuthold, *ACS Photonics* **2017**, *4*, 1371.
[2] N. Li, H. Yuan, L. Xu, J. Tao, D. K. T. Ng, L. Y. T. Lee, D. D. Cheam, Y. Zeng, B. Qiang, Q. Wang, H. Cai, N. Singh, D. Zhao, *ACS Sens.* **2019**, *4*, 2746.
[3] Y. H. Wang, C. P. Chen, C. M. Chang, C. P. Lin, C. H. Lin, L. M. Fu, C. Y. Lee, *Microfluid. Nanofluid.* **2009**, *6*, 333.
[4] J. Wu, Z. X. Wu, H. J. Ding, Y. M. Wei, X. Yang, Z. Y. Li, B. R. Yang, C. Liu, L. Qiu, X. T. Wang, *ACS Appl. Mater. Interfaces* **2019**, *11*, 43383.
[5] A. Harley-Trochimczyk, T. Pham, J. Chang, E. Chen, M. A. Worsley, A. Zettl, W. Mickelson, R. Maboudian, *Adv. Funct. Mater.* **2016**, *26*, 433.
[6] H. Ma, Y. Du, M. Wei, E. Ding, L. Lin, *Sens. Actuators, B* **2019**, *295*, 70.
[7] G. S. Doerk, C. Carraro, R. Maboudian, *ACS Nano* **2010**, *4*, 4908.
[8] D. G. Cahill, P. V. Braun, G. Chen, D. R. Clarke, S. H. Fan, K. E. Goodson, P. Keblinski, W. P. King, G. D. Mahan, A. Majumdar, H. J. Maris, S. R. Phillpot, E. Pop, L. Shi, *Appl. Phys. Rev.* **2014**, *1*, 011305.
[9] J. P. Mathew, R. Patel, A. Borah, C. B. Maliakkal, T. S. Abhilash, M. M. Deshmukh, *Nano Lett.* **2015**, *15*, 7621.
[10] C. Y. Jin, Z. Li, R. S. Williams, K. C. Lee, I. Park, *Nano Lett.* **2011**, *11*, 4818.
[11] T. Kim, Y. W. Kim, H. S. Lee, H. Kim, W. S. Yang, K. S. Suh, *Adv. Funct. Mater.* **2013**, *23*, 1250.
[12] T. B. Song, Y. Chen, C. H. Chung, Y. M. Yang, B. Bob, H. S. Duan, G. Li, K. N. Tu, Y. Huang, Y. Yang, *ACS Nano* **2014**, *8*, 2804.
[13] S. Choi, J. Park, W. Hyun, J. Kim, J. Kim, Y. B. Lee, C. Song, H. J. Hwang, J. H. Kim, T. Hyeon, D. H. Kim, *ACS Nano* **2015**, *9*, 6626.
[14] S. Hong, H. Lee, J. Lee, J. Kwon, S. Han, Y. D. Suh, H. Cho, J. Shin, J. Yeo, S. H. Ko, *Adv. Mater.* **2015**, *27*, 4744.
[15] J.-S. Lee, K.-W. Choi, J.-Y. Yoo, M.-S. Jo, J.-B. Yoon, *Small* **2020**, *16*, 1906845.
[16] K.-W. Choi, M.-H. Seo, J.-S. Lee, K. Kang, I. Park, J.-B. Yoon, *30th Int. Conf. on Micro Electro Mechanical Systems*, IEEE, Las Vegas **2017**, p. 191.
[17] M. H. Seo, J. Y. Yoo, M. S. Jo, J. B. Yoon, *Adv. Mater.* **2020**, *32*, e1907082.
[18] P. Bhattacharyya, *IEEE Trans. Device Mater. Reliab.* **2014**, *14*, 589.
[19] M. Prasad, *Microelectron. Reliab.* **2015**, *55*, 937.
[20] D. C. Xie, D. L. Chen, S. F. Peng, Y. J. Yang, L. Xu, F. Wu, *IEEE Electron Device Lett.* **2019**, *40*, 1178.
[21] H. Long, A. Harley-Trochimczyk, T. Y. He, T. Pham, Z. R. Tang, T. L. Sho, A. Zettl, W. Mickelson, C. Carraro, R. Maboudian, *ACS Sens.* **2016**, *1*, 339.
[22] I. Cho, K. Kang, D. Yang, J. Yun, I. Park, *ACS Appl. Mater. Interfaces* **2017**, *9*, 27111.
[23] A. Rao, H. Long, A. Harley-Trochimczyk, T. Pham, A. Zettl, C. Carraro, R. Maboudian, *ACS Appl. Mater. Interfaces* **2017**, *9*, 2634.
[24] K.-W. Choi, J.-S. Lee, M.-H. Seo, M.-S. Jo, J.-Y. Yoo, G. S. Sim, J.-B. Yoon, *Sens. Actuators, B* **2019**, *289*, 153.
[25] C. S. Prajapati, S. Benedict, N. Bhat, *Nanotechnology* **2020**, *31*, 025301.
[26] Q. Zhou, A. Sussman, J. Chang, J. Dong, A. Zettl, W. Mickelson, *Sens. Actuators, A* **2015**, *223*, 67.
[27] J. Yeon, Y. J. Lee, D. E. Yoo, K. J. Yoo, J. S. Kim, J. Lee, J. O. Lee, S. J. Choi, G.-W. Yoon, D. W. Lee, G. S. Lee, H. C. Hwang, J.-B. Yoon, *Nano Lett.* **2013**, *13*, 3978.
[28] M.-S. Jo, K.-W. Choi, M.-H. Seo, J.-B. Yoon, *Micro Nano Syst. Lett.* **2017**, *5*, 19.
[29] M.-S. Jo, M.-H. Seo, K.-W. Choi, J.-S. Lee, J.-Y. Yoo, H.-J. Song, J.-B. Yoon, *20th Int. Conf. on Solid-State Sensors, Actuators and Microsystems*, IEEE, Berlin **2019**, p. 1694.
[30] M. J. Graf, S. K. Yip, J. A. Sauls, D. Rainer, *Phys. Rev. B* **1996**, *53*, 15147.
[31] F. Volklein, H. Reith, T. W. Cornelius, M. Rauber, R. Neumann, *Nanotechnology* **2009**, *20*, 325706.
[32] F. Biró, C. Dücső, Z. Hajnal, F. Riesz, A. E. Pap, I. Bársony, *Microelectron. J.* **2014**, *45*, 1822.
[33] M. Prasad, P. S. Dutta, *Appl. Phys. A* **2018**, *124*, 788.
[34] J. Spannhake, O. Schulz, A. Helwig, A. Krenkow, G. Muller, T. Doll, *Sensors* **2006**, *6*, 405.
[35] I. D. Kim, A. Rothschild, *Polym. Adv. Technol.* **2011**, *22*, 318.
[36] N. Barsan, M. Schweizer-Berberich, W. Gopel, *Fresenius' J. Anal. Chem.* **1999**, *365*, 287.
[37] C. Wang, L. Yin, L. Zhang, D. Xiang, R. Gao, *Sensors* **2010**, *10*, 2088.
[38] C. O. Park, S. A. Akbar, *J. Mater. Sci.* **2003**, *38*, 4611.